INVESTIGATION OF ONCOMING FLOW CONDITIONS ON THE DYNAMICS OF FLOW OVER A FORWARD-FACING STEP

Emil Larose, Robert Martinuzzi
Department of Mechanical & Manufacturing
Engineering, University of Calgary, Calgary, Canada
louis.larose@ucalgary.ca

Bérengère Podvin, Yann Fraigneau
Laboratoire EM2C & Laboratoire interdisciplinaires
des sciences numériques (LISN), CNRS
Université Paris-Saclay, Orsay, France

Franck Kerhervé
Institut Pprime, CNRS
Université de Poitiers, Poitiers, France

Chris Morton
Department of Mechanical Engineering
McMaster University, Hamilton, Canada

ABSTRACT

Planar, two-component PIV measurements and DNS of thin, laminar and turbulent boundary layers approaching a forward-facing step (FFS) were conducted to investigate the influence of the oncoming flow conditions on intrinsic flow dynamics. Transition of the upstream recirculation bubble between stable and unstable states is shown to be sensitive to small disturbances. The unstable state is characterised by ejections from the upstream bubble resulting in strong interactions with the dynamics of the separated region downstream of the salient edge.

INTRODUCTION

A forward-facing step (FFS) immersed in a fluid flow is a diagnostic flow configuration to investigate fundamental mechanisms of flow instability and separation. It is often encountered in engineering applications such as low-rise buildings and natural landscapes, making this geometry particularly interesting from both scientific and engineering perspectives.

A characteristic of FFS flows is the presence of two separated regions: (i) at the foot of the step due to separation of the oncoming boundary layer (BL) in response to the step-induced adverse pressure gradient, and (ii) immediately downstream of the step due to the sharp corner-induced separation. Bound by the shear layers (SL) and solid boundaries, recirculation bubbles are formed as shown in Figure 1. Many studies have investigated the effects on the topology and dynamics of the flow of the geometry aspect ratios, the thickness of the oncoming BL (δ/H), the flow state and the Reynolds number ($\mathrm{Re}_H = U_\infty H/\nu$). However, little is known about the influence of oncoming flow state on the intrinsic dynamics of FFS flow for thin BL FFS studies ($\delta/H < 1$). This is the principal motivation of this work.

Camussi *et al.* (2008) and Graziani *et al.* (2018) investigated FFS for thick ($\delta/H > 1$) and thin ($\delta/H < 1$) turbulent boundary layers (TBL), respectively. The authors reported that spectral energy content of the wall-pressure fluctuations shifted to lower frequencies as the flow approached the step, indicative of the formation of larger structures at the foot of the FFS. Significant spectral energy content at low frequencies just downstream of the leading edge of the step suggested interactions with the upstream separation. Downstream, structures forming in the SL were related to spectral energy content from initially $f^+ = fH/U_\infty \approx 1$ and decreasing downstream to a band centered around $f^+ \approx 0.2$. This high-frequency band was attributed to the pairing and amalgamation of vortices arising from Kelvin-Helmholtz (KH) instabilities in the separated SL. The low-frequency dynamics of FFS flows are attributed to *flapping* mechanisms of the separation bubbles. At the foot of the step, Graziani *et al.* (2018) found fluctuation energy centred about a frequency of 0.027, while, for thick TBLs, Camussi *et al.* (2008), Pearson *et al.* (2013) and Fang & Tachie (2020) reported frequencies of $f^+ = 0.01$, 0.09 and 0.047, respectively. Similarly, downstream of the step, Graziani *et al.* (2018) and Camussi *et al.* (2008) found a fluctuation frequency of $f^+ = 0.02$, while $f^+ = 0.07$ was reported by Fang & Tachie (2020). In the aforementioned studies, there is general agreement pertaining to the origin of the high-frequency content ($f^+ \approx 0.1$ to 1), while there is no consensus on the characteristic frequencies of the bubble low-frequency motions. The dependence on δ/H suggests that the nature of these low-frequency motions depend on the oncoming flow and associated extrinsic forcing.

The upstream bubble sensitivity to oncoming conditions was shown for an FFS in low-Re_H, laminar channel flow. Wilhem *et al.* (2003) conducted numerical simulations and linear stability analysis demonstrating that the state of the upstream bubble at the foot of the step is sensitive to weak upstream perturbations. They concluded that the transition from a steady large two-dimensional bubble to an unsteady three-dimensional state was not a result of an absolute instability.

For thick TBL, due to large flow perturbations, the upstream bubble is observed in its three-dimensional, unsteady state. Pearson *et al.* (2013) showed that massive fluid ejection events over the step are preceded by low-velocity regions from the oncoming BL that convect over the step. For a very thick TBL, Fang & Tachie (2020) showed that the bubble fluctuations are modulated by large-scale motions (LSM) in the oncoming TBL. Due to the thickness of the BLs in these studies, the LSMs in the BL are the dominant perturbations affecting the FFS flow. Still, to the authors knowledge, little is known about the role of oncoming flow perturbations for thin BLs on the dynamics of the FFS flow.

This study aims to clarify the low-frequency dynamics of FFS flow and their role in the interactions between bubbles. Specifically, the influence of oncoming flow conditions will be evaluated to understand the nature of the underlying, intrinsic dynamics and how they may change with oncoming (extrinsic) forcing such as freestream fluctuations (weak perturbation) or TBL structures (strong perturbations). Hence, an analysis of a breadth of experimental and numerical configurations are considered.

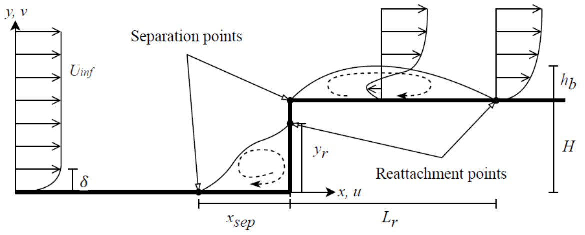

Figure 1. Schematic of the recirculation bubble topology of FFS flow with notations, adapted from Sherry *et al.* (2010).

METHODOLOGY
Experimental

The LTRAC water channel used for the Particle Image Velocimetry (PIV) experiments has a working cross-section of 0.38 m $\times$ 0.5 m, with a working section length of 3 m. At the current water depth, the bulk flow velocity can be set from 0.07 to 0.42 m/s. A FFS model, consisting of a flat plate with an elliptical leading edge with a protruding sharp 90° step ($H =$ 23.6 mm), was suspended in the flume from 4 elliptical struts. No end plates were used, rather there was a 3 mm gap between the model edges and the channel side walls on either side.

Planar, two-component PIV measurements were undertaken with two Phantom Miro 340 cameras, used simultaneously to acquired PIV images, each with a Sigma 65 mm $f/2.8$ DG macro lens, with a native resolution of 2560×1600 pixels^2. The camera sensor sizes were restrained to 2560×856 pixels^2 to increase the number of snapshots per acquisition. Hollow glass spherical particles (specific gravity ≈ 1.1) particles, which seeded the water channel, were illuminated by a thin laser sheet (≈ 2 mm) from a Photonics Industries DM20-527 Nd:YLF dual-cavity laser. The images were processed using LaVision DaVis 10.2 software with a final window size of 12×12 pixels^2 with 50% overlap. Datasets were acquired at sampling frequencies, f_s, of 15 Hz and 100 Hz to resolve low- and high-frequency motions, respectively. Notably, the datasets have proven to show the same dynamics, but only the 15 Hz datasets are shown in this paper for resolution of the low-frequency motions.

As shown in Figure 1, the velocity components are defined as streamwise (u), aligned with the mean freestream (horizontal), and wall-normal (v), perpendicular to the bottom wall (vertical). The origin is the corner at the foot of the step. The scaling parameters are H and U_∞.

Numerical

Direct numerical simulations (DNS) of a LBL and TBL approaching a FFS were performed at LISN, Université de Paris-Saclay (Fraigneau, 2024). The numerical technique is based on an incremental projection method written in rotational formulation to ensure a divergence-free velocity field. The Navier-Stokes equations are discretised in space with a 2$^{\text{nd}}$-order centered scheme. The time discretisation relies on the backward differentiation formula of 2$^{\text{nd}}$ order. A semi-implicit technique on the viscous terms is used to ensure the stability of the numerical method with respect to the time step, which is based on the CFL criterion. Complete details on the numerical method can be found in Faugaret *et al.* (2022).

Table 1. Main oncoming BL properties: thickness δ/H, shape factor δ^*/θ, momentum thickness Reynolds number Re_θ, and state. The properties are extracted at $x/H = -9.5$.

#	Meth.	Re_H	δ/H	δ^*/θ	Re_θ	State
1	PIV	1 700	0.49	2.69	106	Lam.
2	PIV	7 900	0.22	2.69	231	Lam.
3	DNS	8 000	0.38	2.88	384	Lam.
4	PIV	8 100	0.21	1.46	408	Turb.
5	DNS	8 300	0.42	1.65	465	Turb.

The computational domain size is $34H$ (LBL) and $37H$ (TBL) $\times \pi H \times 22H$ in the streamwise, spanwise and wall-normal directions, respectively. The step is placed $14H$ (LBL) and $17H$ (TBL) downstream from the inlet. The boundary conditions are defined as the usual no-slip conditions at walls, stress-free and zero mass flow rate conditions at the top of the domain and periodic conditions in the spanwise direction. In one case, the inlet flow is a Blasius profile of with $\delta/H = 1/3$. In the other case, the inlet flow is a TBL characterized by statistical turbulent profiles at $\mathrm{Re}_\theta = 300$ (Spalart, 1988). Turbulent fluctuations are mimicked with a synthetic eddy model (Deck & Laraufie, 2013).

The Cartesian grid is made up of $1920 \times 384 \times 768$ cells. The grid spacing in the streamwise direction varies between 4.5+ and 12.5+ wall units, with a minimum value in the vicinity of the step. In the spanwise direction, the spacing is uniform at approximately 3.7+. Finally, the grid spacing evolves between 0.3+ and 4.7+ in the wall-normal direction over one step height from the wall. The time step is set to 4.5×10^{-4} time units in order to satisfy a CFL value less than 0.4 over the range of the entire domain. Data have been recorded over a time range of 200 and 400 time units for the LBL and TBL, respectively.

FLOW CASES

The cases of interest are summarised in Table 1. They were chosen such to investigate the FFS flow dynamics for a variety of oncoming flow conditions. Namely, laminar boundary layer (LBL) cases with and without freestream disturbance (cases 1 & 3), LBL cases below and above a critical Re_H (cases 1 & 2) with disturbance, and TBL cases with and without freestream disturbance (cases 4 & 5).

The time-averaged streamwise velocity ($\overline{U}$) profiles at $x/H = -9.5$ for the LBL cases (1, 2 & 3) exhibit strong agreement with Blasius' solution for the LBL profile as shown in Figure 2. It is important to underscore that this inflow parameter is the same across all laminar cases in this study regardless of the Re_H and freestream disturbance level. Although the BL thickness is not constant across these cases, they remain thin compared to H ($\delta \leq 0.5H$ for all cases). The LBL profiles along with the quantities in Table 1 indicate that the oncoming flow can be characterized as laminar for cases 1 & 2, namely $\mathrm{Re}_\theta < 300$ and $\delta^*/\theta \approx 2.62$ (Smits, 2010). In the case of the LBL DNS, case 3, an inflection in the $\overline{U}$ profile is observed. As a result, both Re_θ and δ^*/θ are greater than expected for a LBL. Regardless, the inflow condition remains a LBL.

The TBL profiles along with the quantities in Table 1 indicate that the oncoming BL for cases 4 & 5 can be characterized as turbulent. The freestream velocity fluctuation intensity is estimated to be 1.3% for all experimental PIV measurements.

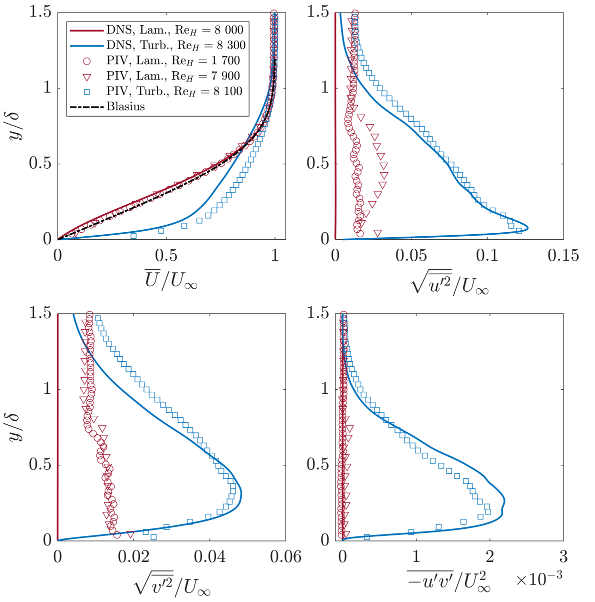

Figure 2. Oncoming BL profiles of the mean streamwise velocity, the streamwise and wall-normal velocity fluctuation intensity, and the Reynolds shear stresses. The profiles are extracted at $x/H = -9.5$.

MEAN FLOW CHARACTERISTICS

The time-averaged streamwise velocity and the in-plane Reynolds shear stresses are examined to characterize the mean flow field structure and highlight regions of interest (Figure 3).

TBL cases (4 & 5): The velocity and shear stress profiles are nearly identical in distribution and magnitude for both PIV and DNS configurations, which suggests similarities in the underlying flow physics. Consistent with Sherry *et al.* (2010), for comparable Re_H and δ/H the FFS flow with a TBL is insensitive to freestream disturbances. The upstream bubble is small with the mean upstream separation and step wall reattachment at $x_{sep} \approx -0.6H$ and $y_r \approx -0.65H$, respectively. The downstream bubble height and reattachment lengths are $h_b \approx 0.4H$ and $L_r \approx 3.5H$ & $4.3H$, respectively.

LBL cases (1 & 3): From Figure 3(a), the $\overline{U}$ profiles nearly overlap for these cases. These demonstrate a large upstream recirculation bubble with upstream flow separation at $x_{sep} \approx -6H$ and reattachment on the step face at $y_r \approx 0.75H$ & $0.9H$, respectively. A pronounced inflection of the BL upstream of the step is observed, which hints at a susceptibility to instability. However, the negligible magnitude of the shear stresses upstream suggest that transition has not occurred. Downstream of the step, the bubble height and reattachment lengths are $h_b \approx 0.3H$ and $L_r \approx 3.75H$ & $2.5H$, respectively. In both cases, laminar flow separation occurs at the salient edge of the FFS. The growth of the shear layer (SL) instability leads to transition and subsequent vortex shedding at the tail of the downstream recirculation bubble. In Figure 3(b), the instability growth process contributes to increased shear stresses at $x \geq 2H$ & $1H$, respectively. Discrepancies between these cases are believed to be Re_H effects. As case 3 exhibits a sharper streamwise velocity gradient in the wall-normal direction ($\frac{\partial U}{\partial y}$), greater susceptibility to SL instability and transition is expected. Based on these observations, in case 3 flow transition and TBL reattachment occurs closer to the step than case 1, leading to a smaller L_r on the top of the step.

In case 2, upstream flow separation and step wall reattachment occur at $x_{sep} \approx -0.65H$ and $y_r \approx 0.65H$, while the downstream bubble height and reattachment length are $h_b \approx 0.3H$

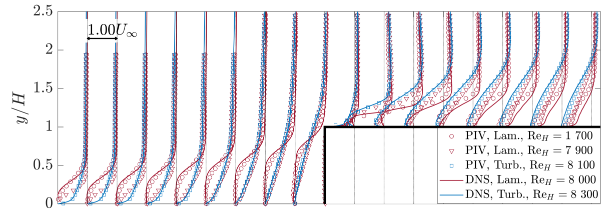

(a) $\overline{U}/U_\infty$

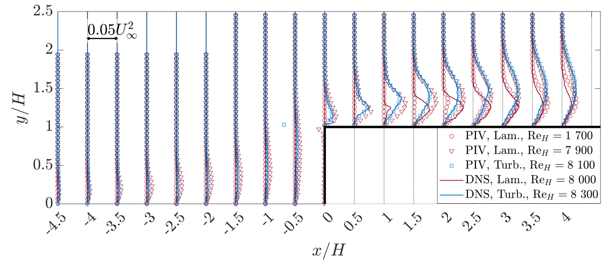

(b) $-\overline{u'v'}/U_\infty^2$

Figure 3. The mean streamwise velocity and Reynolds shear stress profiles. Every 4^{th} marker is indicated for the PIV data.

and $L_r \approx 3.5H$. These metrics are thus, unexpectedly, comparable to TBL cases 4 & 5 while the oncoming BL is laminar. Close examination of the instantaneous velocity snapshots reveals that a transition in the state of the bubble at the foot of the step in case 2 occurs. In cases 1 & 3, the upstream bubble is steady, while in case 2 (similarly to cases 4 & 5) the upstream bubble exhibits unsteady behaviour. This occurs despite (i) an oncoming LBL with disturbance conditions comparable to case 1 and (ii) a comparable Re_H to case 3. However, for case 2, the BL is excited by the freestream disturbances and these perturbations are believed to be convected downstream, triggering a transition in the recirculation at the foot of the step. For a specific disturbance level, we suggest that there exists a critical Re_H at which this bubble becomes unstable. While not reported here for brevity, similar receptivity phenomena were observed for experiments conducted at $Re_H = 4\,800$. This critical Re_H number may therefore lie between 1 700 and 4 800, for this experimental setup. Note that the Re_H number of the DNS case 3 is well-beyond this critical number. Therefore, a similar behavior could be expected. However, for this case, there is no source of disturbance that may trigger the bubble instability.

In the following, we turn to the Proper Orthogonal Decomposition (POD) (Sirovich, 1987). Since POD is defined using an energetic criteria and the flow downstream of the step contains most of the velocity fluctuation energy, it is applied in two domains separately: upstream ($-5 \leq x/H \leq 0$ & $0 \leq y/H \leq 2$) and over the full domain ($-5 \leq x/H \leq 4.25$ & $0 \leq y/H \leq 3$). Note that both u' and v' are considered in solving the eigenvalue problem. In the following sections, the spatial eigenmodes and temporal eigenfunctions obtained are examined and discussed in detail.

FLOW UPSTREAM OF THE STEP

The modal energy distribution for the upstream domain is presented in Figure 4(a). The distribution for TBL cases 4 & 5 match closely, further supporting the similarity between the PIV and DNS results. Consistent with the Reynolds stresses in Figure 3(b), the total turbulent kinetic energy (TKE) of the POD modes for these two cases is more than two orders of magnitude greater than that for the LBL cases 1 & 3. For the latter two cases, the cumulative energy content increases more rapidly (see inset in Figure 4(a)): the first 20 modes represent

96% of the TKE, while for the TBL cases the same number of modes capture less than 50% of the TKE. Also consistent with Figure 3(b), case 2 exhibits larger modal energy. The cumulative energy distribution for this case is comparable to that of the two TBL cases, further indicating similarity with the TBL cases despite the LBL inflow.

The POD spatial modes 1, 2, 3, and 5, and associated power spectral density function estimates (PSDF) of the temporal coefficients are shown in Figure 5. Modes 4 and 5 have similar energy content, but mode 5 highlights the dynamics of interest. Results obtained for the TBL PIV and DNS cases (columns 5 & 6) are similar. The first two modes indicate an oscillatory motion immediately near the step with a characteristic length scale of $2H$, and spectral energy content centered around $f^+ \approx 0.07$. The spatial organisation of the four first modes suggest fluid ejection from the upstream bubble over the step, as observed by Pearson *et al.* (2013) for a thick TBL ($\delta/H > 1$). Both cases 4 & 5 may therefore be associated with an unsteady upstream bubble due to the oncoming TBL. The shift of the spectral energy to $f^+ \approx 0.1$ and shorter wavelengths in the spatial modes for modes 3 and 5 suggests convective dynamics associated with ejection from the bubble.

For cases 1 & 3 (columns 1–3), a weak, low-frequency oscillation of the upstream bubble is observed along with spectral energy content at $f^+ \approx 0.03$. The natural frequency of the water channel is in this range for case 1 ($f_n = 0.086$ Hz at all flow speeds), causing a more pronounced peak in the PSDF. For this case, modes 3 & 5 exhibit a pronounced spectral energy concentration at $f^+ \approx 0.15$. Note: the peak in the PSDF of mode 5 is exaggerated due to scaling by the a very small variance value (σ^2). It is believed that these modes with strong spectral content at $f^+ \approx 0.15$ are the excitation of the natural bubble instability – precursor to transition to an unsteady upstream bubble – because similar spatial mode and spectral energy content is seen for cases 2, 4 & 5, where the upstream bubble is unsteady. Unlike case 2, however, the excitation of the upstream bubble is insufficient to trigger transition to an unsteady recirculation bubble. While the DNS data does not fully resolve the low frequencies (due to limited duration of the dataset), the PSDFs are consistent with those of case 1 in the band $f^+ < 0.1$. Spectral energy at $f^+ \approx 0.15$ is found in higher ranked POD modes of case 3 due to the absence of disturbances to excite the instability of the bubble.

The spatial POD modes for case 2 (column 4) closely match that for the TBL cases 4 & 5. This confirms that the transition of steady to unsteady bubble governs the flow dynamics at the foot of the step. The transition itself is governed by oncoming disturbances and Re_H.

FLOW DOWNSTREAM AND OVER THE STEP

To highlight connections between the upstream and downstream flow dynamics, the POD is applied to the full domain. The modal energy distribution, presented in Figure 4(b), shows the agreement between cases 4 & 5 (TBL). The energy distribution obtained for case 2 is comparable with that of these two cases, as shown in the cumulative energy distribution (inset of Figure 4(b)). The energy distribution of cases 1 & 3 are quite different. The cumulative distribution of case 1 converges more quickly: the first 20 modes represent 80%, while they represent only 50% of the energy in case 3.

The first 5 spatial modes and associated PSDFs are presented in Figure 6. For cases 2, 4 & 5 (columns 4 to 7), mode 1 can be associated with the low-frequency flapping instability or *breathing* – expansion and contraction – of the downstream bubble (Sherry *et al.*, 2010) resulting in the spectral signature at $f^+ \approx 0.04$. The subsequent modes arise in pairs and emphasise the development of coherent motions which convect along the downstream SL. The spectral energy content of that modes shifts from $f^+ \approx 0.15$ in mode 2 to $f^+ \approx 0.3$ in mode 4 while the characteristic wavelength is reduced. The ejection of fluid over the step is manifested in modes 3 & 4 for case 2 and in modes 5 & 6 (the latter is not shown for brevity) for cases 4 & 5. These modes are characterised by an additional low-frequency content at $f^+ \approx 0.07$, which is also observed in the PSDFs of the upstream POD modes in Figure 5. This observation indicates an interaction between the upstream and downstream bubbles. The fluid ejections act on the downstream SL, thereby modulating its flapping as well as the shedding mechanism.

For cases 1 & 3, the first two POD modes (columns 1 & 2 of Figure 6) appear to be a mode pair representing a travelling pattern. From the PDSFs (column 3), the dominant shedding frequency is $f^+ \approx 0.17$, which is very close to $f^+ \approx 0.15$ observed in the upstream domain. It is thus proposed that the oscillation of the upstream bubble is imprinted on the oncoming flow, which in turn modulates the SL separating from the step corner. Modes 3 to 5 exhibit a reduced wavelength over the step and increased peak frequency. These appear related to the downstream shedding process. In contrast to TBL case 4 & 5, a mode associated with *breathing* of the downstream bubble is not observed. Cases 1 & 3 exhibit laminar flow separation at the step, SL instability growth and subsequent transition to turbulent vortex shedding.

The flapping instability of the downstream SL appears to be related to the upstream bubble transition to an unsteady state. As pointed out previously, POD modes of case 2 (column 4) in the upstream region closely match those of the TBL cases. The transition to an unsteady upstream bubble brought upon by the excitation of the BL leads to flow dynamics over the step being similar to that observed with an oncoming TBL.

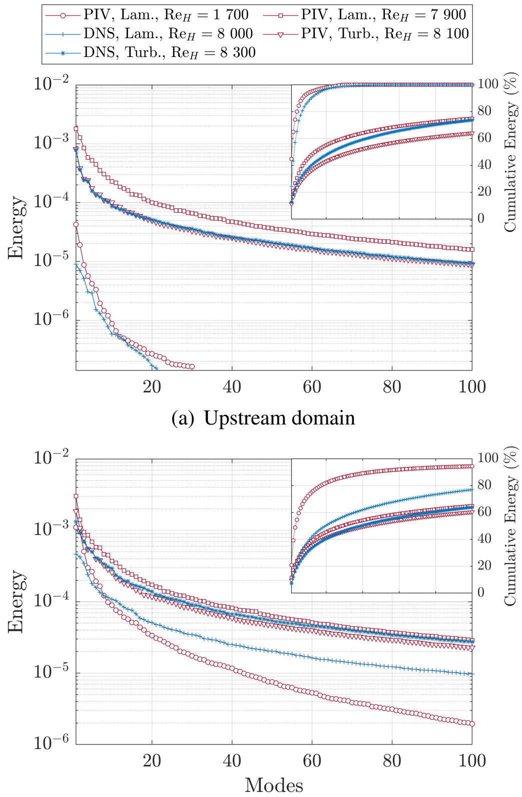

(a) Upstream domain

(b) Full domain

Figure 4. POD modal energy distribution for both domains for all cases. Inset is the cumulative energy distribution.

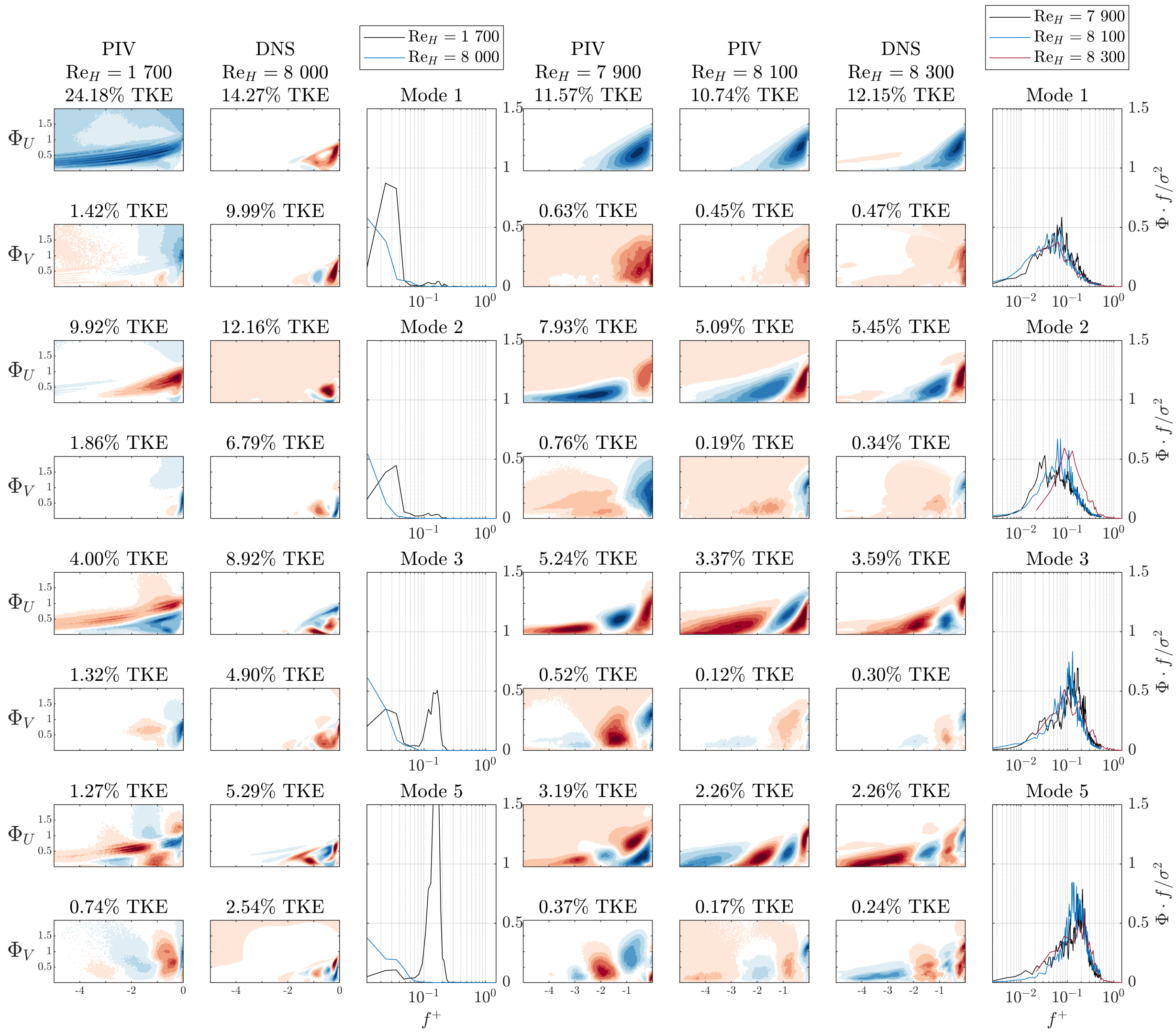

Figure 5. Leading POD spatial modes of the upstream domain with the associated PSDF of the temporal coefficients. Columns indicate the cases and every 2-row combination corresponds to a mode number. Every row therein corresponds to a velocity component.

The interactions between upstream and downstream bubbles are highlighted by modes 3 to 5. Note: these interactions appear similar, but in lower ranked modes in cases 4 & 5. These dynamics are not observed in cases 1 & 3. Therefore, if the oncoming LBL is excited by disturbances and the Re_H is sufficiently high, the upstream bubble becomes unsteady and the FFS flow dynamics resemble that of a TBL. As such, the oncoming BL alone is not an adequate predictor for FFS flow.

CONCLUSIONS

A systematic survey of FFS flow with different inflow conditions is conducted in this work using numerical data (DNS) and experimental (PIV) data. Three scenarios have been identified with regards to the upstream bubble dynamics. *Firstly*, an unsteady recirculation bubble upstream of the step is observed for TBL (cases 4 & 5). The ejection of fluid over the step at $f^+ \approx 0.07$ is found to be a dominant motion. *Secondly*, when the upstream bubble oscillates weakly about a steady state (cases 1 & 3), the dominant dynamics are related to the long time scale oscillation of the bubble ($f^+ \approx 0.03$). In addition, if the bubble is subjected to oncoming disturbances, the bubble instability is excited ($f^+ \approx 0.15$) without transition. *Third*, despite a LBL inflow, above a critical Re_H and perturbation level, transition to an unsteady bubble state at the foot of the step is observed (case 2). Then, the dynamics are comparable to that observed for TBLs.

The dynamics of the recirculation bubble at the foot of the step has been found thus to lead to two scenarios for flow over the step. *First*, when the upstream bubble is unsteady (cases 2, 4 & 5), turbulent separation, vortex shedding, SL flapping and convective interactions have been observed. The instability of the separated SL from the oncoming turbulent flow results in a vortex pairing and amalgamation process that leads to the shedding of large structures from the downstream bubble ($f^+ \approx 0.1 - 0.3$). This motion is found to be coupled to a low-frequency flapping instability of the downstream bubble ($f^+ \approx 0.04$). Importantly, a convective interaction between the bubbles is also found to occur from the ejection mode of the bubble at the foot of the step. *Secondly*, when the upstream bubble is in a steady state (cases 1 & 3), steady laminar separation and vortex shedding are observed over the step. The instability of the SL grows further downstream from the edge of the step until a breakdown into turbulent flow and vortex shedding occurs. In this situation, no convective interaction between the bubbles has been identified.

REFERENCES

Camussi, R., Felli, M., Pereira, F., Aloisio, G. & Di Marco, A. 2008 Statistical properties of wall pressure fluctuations over a forward-facing step. *Physics of Fluids* **20** (7), 075113.

Deck, Sébastien & Laraufie, Romain 2013 Numerical investi-

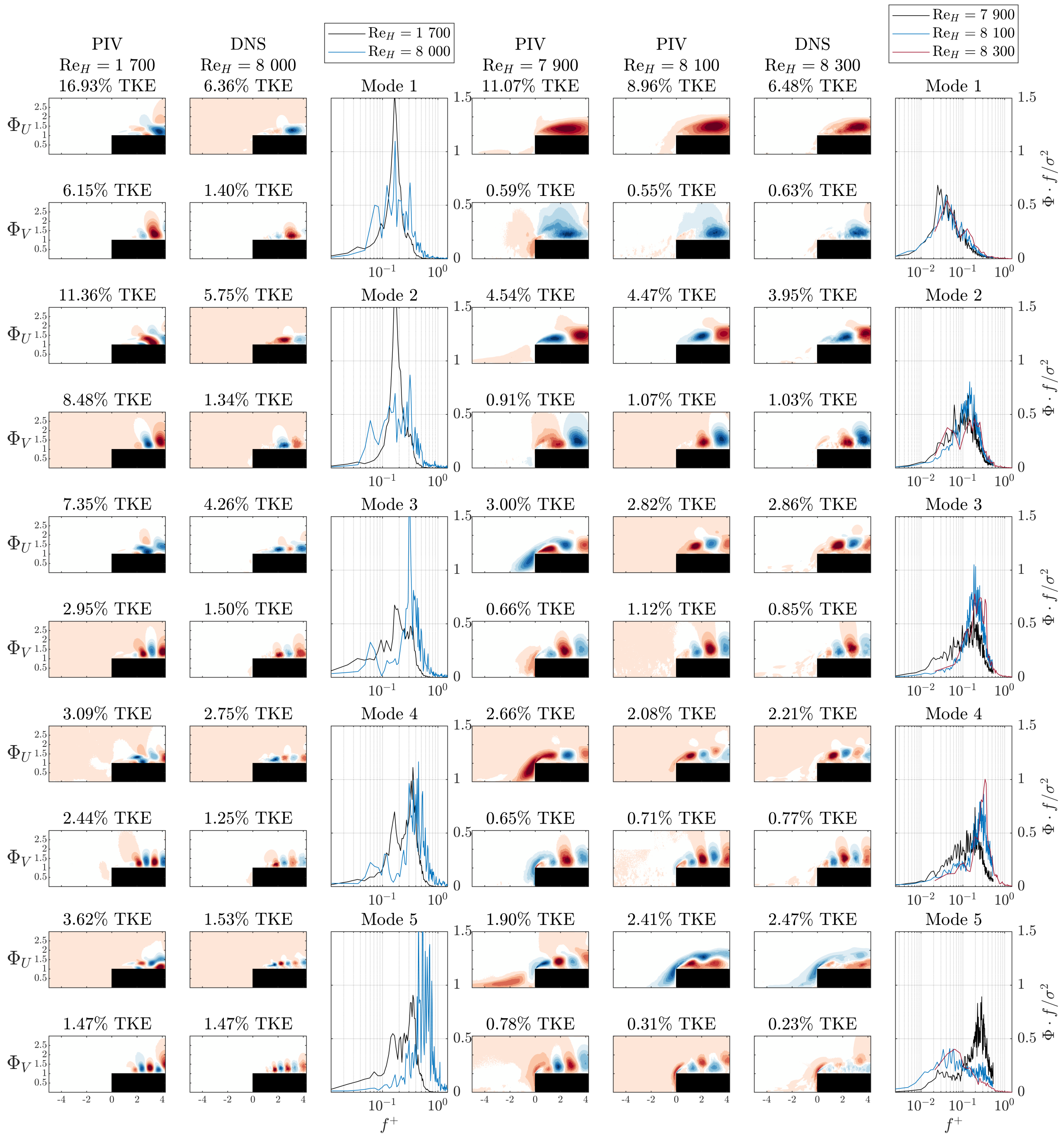

Figure 6. Leading POD spatial modes of the full domain with the associated PSDF of the temporal coefficients.

gation of the flow dynamics past a three-element aerofoil. *Journal of Fluid Mechanics* **732**, 401–444.

Fang, Xingjun & Tachie, Mark F 2020 Spatio-temporal dynamics of flow separation induced by a forward-facing step submerged in a thick turbulent boundary layer. *Journal of Fluid Mechanics* **892**, A40.

Faugaret, A., Duguet, Y., Fraigneau, Y. & Martin-Witkowski, L. 2022 A simple model for arbitrary pollution effects on rotating free-surface flows. *Journal of Fluid Mechanics* **935**.

Fraigneau, Yann 2024 DATABASE-FLMEC : a CFD database on unsteady and turbulent flows.

Graziani, A., Kerhervé, F., Martinuzzi, R. J. & Keirsbulck, L. 2018 Dynamics of the recirculating areas of a forward-facing step. *Experiments in Fluids* **59** (154), 1–18.

Pearson, D. S., Goulart, P. J. & Ganapathisubramani, B. 2013 Turbulent separation upstream of a forward-facing step. *Journal of Fluid Mechanics* **724**, 284–3042.

Sherry, M., Jacono, D. Lo & Sheridan, J. 2010 An experimental investigation of the recirculation zone formed downstream of a forward facing step. *Journal of Wind Engineering & Industrial Aerodynamics* **98** (12), 888–894.

Sirovich, Lawrence 1987 Turbulence and the dynamics of coherent structures. i. coherent structures. *Quarterly of applied mathematics* **45** (3), 561–571.

Smits, Alexander J. 2010 Viscous flows and turbulence. In *Lectures in Fluid Mechanics*. Princeton University.

Spalart, Philippe R. 1988 Direct simulation of a turbulent boundary layer up to rtheta = 1410. *Journal of Fluid Mechanics* **187**, 61–98.

Wilhem, Dirk, Härtel, Carlos & Kleiser, Leonhard 2003 Computational analysis of the two-dimensional–three-dimensional transition in forward-facing step flow. *Journal of Fluid Mechanics* **489**, 1–27.